Halloysite Nanotube Reinforced Biodegradable Nanocomposites Using Noncrosslinked and Malonic Acid Crosslinked Polyvinyl Alcohol

Kaiyan Qiu, Anil N. Netravali
Fiber Science Program, Cornell University, Ithaca, New York 14853-4401

Halloysite nanotubes (HNTs) based thin membrane-like fully biodegradable nanocomposites were produced by blending individualized HNT dispersion with polyvinyl alcohol (PVA). Stable individualized HNT dispersion was obtained using several separation techniques, sequentially, prior to blending with PVA. PVA was crosslinked using malonic acid (MA) as crosslinker and phosphoric acid as catalyst, to increase the mechanical and thermal properties of HNT–PVA nanocomposites. Crosslinking was also intended to make PVA water-insoluble and hence more useful in commercial applications. Examination of the composites indicated that HNTs were uniformly dispersed in both PVA as well as crosslinked PVA. Excellent mechanical properties of the HNT–PVA nanocomposites were achieved. These nanocomposites are intended to be composted at the end of their life rather than ending up in landfills as most of today's traditional petroleum based non-biodegradable plastics. POLYM. COMPOS., 34:799–809, 2013. © 2013 Society of Plastics Engineers

INTRODUCTION

During the past decade or so polymer property modifications using nanoparticles and formation of nanocomposites has seen significantly increased interest. There are several reasons why nanoparticles with nanometer scale dimensions (10^{-9} m) are of interest. Nanoparticles with such small dimensions have been shown to improve not only the mechanical properties of polymers but also, in many cases, their functionalities as well [1–5]. In addition, only small loading of nanoparticles is sufficient to obtain significant property changes.

Halloysite nanotubes (HNTs) based on aluminosilicate clay nanosheets that are naturally rolled to form hollow tubular structures are mined from natural deposits [6, 7]. While the ideal unit formula for halloysite is $Al_2Si_2O_5(OH)_4 \cdot nH_2O$ [$n = 0$ for halloysite (7 Å) and $n = 2$ for hydrated halloysite (10 Å)], the chemical composition is subject to variation due to the presence of impurities such as Fe oxides [7]. Halloysite has been found to occur widely throughout the world in weathered rocks as well as in soils and has been identified as having formed by the alternation of a wide variety of igneous and non-igneous rocks [6–8]. It is often intermixed with dickite, kaolin, montmorillonite, and other clay minerals [8]. Since the dominant morphology of halloysite is tubular, it is commonly termed as HNTs [7]. Unlike other nanostructured clays that must be exfoliated, HNTs naturally occur as cylinders with average diameters typically smaller than 100 nm and lengths ranging from 500 nm to over 1.2 μm [8]. HNTs have been used as bioreactors, time-release capsules, catalysts of polymer degradation, templates for depositing other nanoparticles, polymer filler, or property modifier as well as in ceramic applications [6].

HNTs have been widely used during recent years to reinforce polymers and resins such as epoxy, polypropylene, polyamide, styrene rubber, and ethylene propylene diene monomer rubber [9–18]. Although such nanocomposites possess good mechanical and thermal properties, they are not biodegradable and need to be disposed of in landfills at the end of their life [9–18]. In the case of "green" biodegradable soy protein based resin the addition of HNTs was shown to improve its fire resistance [19].

Polyvinyl alcohol (PVA) is a thermoplastic and biocompatible petroleum based polymer. It is also one of the rare polymers with a carbon–carbon single bond backbone that is fully biodegradable [20]. Because of the hydroxyl (–OH) groups on alternating carbon atoms PVA is strongly hydrophilic and soluble in water, which helps to promote its degradation through hydrolysis [20]. However, PVA has relatively low strength and thermal stability for some applications. Fabricating biodegradable HNT–PVA nanocomposites may be a potential way to address some limitations of the PVA. Such nanocomposites can have excellent mechanical properties and thermal stability because the HNTs are stable even at very

Correspondence to: Anil N. Netravali; e-mail: ann2@cornell.edu
Contract grant sponsor: National Textile Center (NTC) and the Wallace Foundation.
DOI 10.1002/pc.22482
Published online in Wiley Online Library (wileyonlinelibrary.com).

high temperatures [19]. HNT–PVA nanocomposites have been reported earlier but without proper HNT individualization and any PVA modifications [21, 22]. The present research shows that individualized HNT addition together with crosslinking of PVA can achieve significantly better properties.

Crosslinking has been commonly used to improve the mechanical and thermal properties as well as reduce solubility of many polymers [23–27]. When used as resin, crosslinked polymers can also improve composite properties. Crosslinking is a process of chemically joining two or more molecules at different locations along their length by covalent bonds. Crosslinkers are commonly selected on the basis of their chemical reactivities with the functionalities present on the polymers [23]. Glutaraldehyde and glyoxal are two universally used crosslinkers for polymers that contain amine groups such as proteins [24–26]. Although both of them are effective in crosslinking polymers, they are relatively toxic [27]. Therefore, less toxic crosslinkers are of interest in the crosslinking reaction, particularly to maintain the biodegradability of the polymers.

Malonic acid (MA) is a dicarboxylic acid produced from chloroacetic acid and can be used as a crosslinker [28]. In terms of toxicity, it is a much better choice as a crosslinker than glutaraldehyde or glyoxal [27]. Some researchers have shown crosslinking of PVA using dicarboxylic acids, including MA, with sulfuric acid as catalyst to obtain esterification [29, 30]. However, the effectiveness of crosslinking has not been as good as expected and, importantly, the mechanical and thermal properties of PVA after crosslinking were not investigated in these studies.

In this study, HNT clusters were individualized using several techniques and membrane-like biodegradable HNT–PVA nanocomposites were fabricated and their properties characterized. PVA and HNT–PVA nanocomposites were crosslinked using MA, with phosphoric acid as catalyst. High crosslinking levels of PVA and PVA in HNT–PVA nanocomposites were achieved making PVA water-insoluble. In addition, HNT loading in nanocomposites could be easily controlled as desired. These thin membrane-like nanocomposites had smooth surfaces and their tensile and thermal properties were excellent. The MA crosslinked HNT–PVA nanocomposites showed even better properties.

MATERIALS AND METHODS

Individualization of HNTs

HNT powder was initially added into deionized water at a weight ratio of 1:49. Tween® 80 [Sigma-Aldrich, St. Louis, MO; HNT:Tween® 80 (w/w)=10:1] was then added into the mixture, as non-ionic surfactant, to help individualize the HNTs. The pH value of the mixture was adjusted to 10 to further avoid clustering of HNTs [8]. The mixture (at pH = 10) was stirred using mechanical stirrer (Polymix®, PX-SR 90 D, Kinematica Inc., Bohemia, NY) at 90°C and 1000 rpm for 1 h and followed by ultrasonication (Branson Ultrasonics, Model 2510, Mumbai, India) at 65°C for 1 h to form original HNT dispersion. The original HNT dispersion was kept standing for 2 days until it was stabilized. The supernatant of the HNT dispersion was used as final individualized HNT dispersion while the solution at the bottom containing HNT deposition was removed. The HNT content in the final individualized HNT dispersion was 0.5% by weight. The 0.5% HNT content in HNT dispersion was found reproducible and experimentally controllable as this experiment was conducted over five times and the same results were obtained.

Preparation of PVA and Crosslinked PVA Using MA

PVA powder (M_w 31,000–50,000, 98–99% hydrolyzed, Aldrich, St. Louis, MO) was added to the deionized water at a weight ratio of 1:9 to form PVA solution which was maintained in a water bath at 80°C and stirred for 30 min. MA powder (ReagentPlus®, 99%, Sigma-Aldrich, St. Louis, MO) was then added to the PVA solution. The weight ratio of MA and PVA was 1:10. The pH value of the mixture was adjusted to 1 by adding phosphoric acid (85 wt% solution in water, Mallinckrodt Baker, Phillipsburg, NJ). The mixture was stirred at 90°C for 1 h for precuring. The precured mixture was then cast on Teflon® coated glass plates and slowly dried in an oven at 40°C to form flat precured crosslinked PVA film. The precured film was further hot pressed at 100°C under a pressure of 0.2 MPa for 60 min to form cured crosslinked PVA film. Carboxylic ester linkages are expected to form between hydroxyl group of PVA and carboxylic groups of MA at high temperature during the hot pressing [29, 30]. The cured (crosslinked) PVA film was then immersed into deionized water at RT for 12 h until the system got stabilized in order to partially remove phosphoric acid, remaining MA, and noncrosslinked PVA. The water-immersed and cured crosslinked PVA film was then dried at 40°C to form final crosslinked PVA film. The PVA film was prepared by casting PVA solution without the addition of MA as control, for comparison.

Fabrication of HNT-PVA Nanocomposites

The PVA solution (10% by weight) was added to the final individualized HNT dispersion at desired PVA and HNT weight ratios. The HNT dispersion and PVA solution mixtures were stirred at 90°C for 1 h. The mixtures were cast on Teflon® coated glass plate and slowly dried in an oven at 40°C to form HNT–PVA composite sheets (5, 10, and 20 HNT loading, by weight, in the composites). The HNT–PVA nanocomposite sheets were hot pressed at 100°C and 0.2 MPa for 60 min to form the final nanocomposites.

 DOI 10.1002/pc

Preparation of Crosslinked HNT–PVA Nanocomposites Using MA

The 10% (by weight) PVA solution was added to the final individualized HNT dispersion at desired PVA and HNT weight ratios. The HNT dispersion and PVA solution mixtures were stirred at 90°C for 1 h and ultrasonicated at 65°C for 1 h. MA powder (ReagentPlus®, 99%, Sigma-Aldrich, St. Louis, MO) was then added to the mixtures. The weight ratio of MA to PVA was 1:10. The pH values of the mixtures were adjusted to 1 by adding crosslinking catalyst phosphoric acid (85 wt% solution in water, Mallinckrodt Baker, Phillipsburg, NJ). The mixtures were stirred at 90°C for 1 h for precuring. The precured mixtures were then cast on Teflon® coated glass plates and slowly dried in an oven at 40°C to form flat precured crosslinked HNT–PVA nanocomposites (5, 10, and 20% HNT loading, by weight, in the nanocomposites). The precured composites were further hot pressed at 100°C under a pressure of 0.2 MPa for 60 min to form crosslinked HNT–PVA nanocomposites as stated earlier. The crosslinked HNT–PVA nanocomposites were then immersed into deionized water at RT for 12 h until the system got stabilized in order to partially remove phosphoric acid, remaining MA, and noncrosslinked PVA. The water-immersed and cured crosslinked HNT–PVA nanocomposites then dried at 40°C to form final crosslinked HNT–PVA nanocomposites with an average thickness of 0.5 mm.

Characterization

TEM and SEM Analysis. HNT–PVA nanocomposites (10% HNT loading) and MA crosslinked HNT–PVA nanocomposites (10% HNT loading) were initially frozen by liquid nitrogen and then cut into thin sections (40–100 nm thickness) using microtome (Leica EM UC7/FC7 Cryoultramicrotome, Leica Microsystems, Cambridge, UK) with a diamond cutter. The thin sections of HNT–PVA nanocomposites were observed with transmission electron microscopy (FEI Tecnai™ F20 TEM, FEI Company, Hillsboro, OR). Copper grids with 300 mesh size were used to hold the specimens for TEM.

HNT–PVA nanocomposites (10% HNT loading) were also sputter coated with gold to prevent charging and improve the image contrast. Their surface topographies were observed using a scanning electron microscope (SEM Leica 440, Leica Microsystems, Cambridge, UK) at an accelerating voltage of 15 kV.

Sol–Gel and Swelling Analyses. PVA and MA crosslinked PVA specimens (crosslinked PVA film and the crosslinked resin in HNT–PVA nanocomposites, 10% HNT loading) were fully dried at 105°C for 12 h prior to conducting the sol–gel test. The specimens were weighed to obtain their initial dry weights and then immersed in distilled water in 150 mL glass bottles. The glass bottles with the specimens were then placed on a shaker table (MAXQ 4450, Thermo Scientific, Waltham, MA) maintained at 80°C and 150 rpm for 2 h until the control (noncrosslinked) PVA was completely dissolved. The remaining solid contents for the crosslinked specimens were then washed three times with distilled water and filtered using a Whatman® filter paper (Number 4, 20–25 μm pore size) to obtain final residues. The water soluble portion (sol) and particles smaller than the pore size of the filter paper were removed. The final residues of the crosslinked PVA and the crosslinked HNT–PVA nanocomposites were dried at 105°C for 12 h to obtain their dry weight (gel). Ratios of the dry gel weight of the crosslinked PVA to their corresponding initial dry weight were used to determine the PVA gel (crosslinked) percentages. The HNT weight in the crosslinked HNT–PVA nanocomposites were regarded as constant before and after the test.

PVA and MA crosslinked PVA specimens (crosslinked PVA film or the crosslinked resin in HNT–PVA nanocomposites, 10% HNT loading) were dried at 105°C for 12 h prior to conducting the swelling test. The specimens were weighed to obtain their initial dry weight and then immersed in distilled water in 150 mL glass bottles at RT for 24 h. The surface water from the swollen specimens was wiped using Kimwipe® paper tissue to remove excess water weighed again to obtain the swollen weight. Ratios of the weight of absorbed water by the specimens to their corresponding initial dry weight were used to determine the swelling power of the control and crosslinked PVA. The HNT weight in the crosslinked HNT–PVA nanocomposites was regarded as constant, before and after the test.

ATR-FTIR Spectroscopy. Chemical analysis of HNT–PVA nanocomposites (10% HNT loading) and its MA crosslinked specimens was carried out using FTIR spectrophotometer (Nicolet Magna-IR 560, Thermo Scientific, Waltham, MA) in attenuated total reflection (ATR) mode using a split pea accessory. Spectra, averaged over 64 scans, were taken in the range of 4000–800 cm^{-1} wavenumber at a resolution of 4 cm^{-1}. All nanocomposite specimens were dried in an air circulating oven at 40°C for 12 h prior to conducting the spectroscopy. The surface chemistry (ATR-FTIR) and the bulk chemistry (of the cross-section) of crosslinked PVA were found to be identical confirming that there was no difference between the surface and the bulk chemistry.

Tensile Properties and Moisture Content. The specimens for PVA, HNT–PVA nanocomposites (5, 10, and 20% HNT loading) and their corresponding crosslinked specimens were cut to 10 mm × 60 mm strips and were tensile tested using an Instron universal testing machine (model 5566). These tests were conducted as per ASTM D-882-02. Specimen gauge length of 30 mm and strain rate of 0.02/min were used for all specimens. Specimens

were conditioned at 21°C and 65% RH for 3 days prior to testing.

Percentage moisture content (MC%) for all conditioned specimens were measured as per ASTM D 2654-89a. To obtain the MC% values specimens were dried in an oven at 105°C until their weight stabilized. The MC% values were calculated on the dry weight basis.

Thermogravimetric Analysis (TGA). Thermogravimetric analysis (TGA Model Q500, TA Instrument, New Castle, DE) was used to characterize the thermal degradation behavior of all specimens. Specimens were dried in an air circulating oven at 45°C for 12 h prior to conducting the tests. All TGA tests were performed between 25 and 800°C under a nitrogen atmosphere (gas flow rate of 60 mL/min) and at a scanning rate of 10°C/min.

Differential Scanning Calorimetry (DSC). Differential scanning calorimetry (DSC, Model Q2000, TA Instrument, New Castle, DE) was used to analyze the glass transition temperature (T_g), melting temperature (T_m), enthalpy of fusion (ΔH_f) and crystallinity of PVA, HNT–PVA nanocomposites (10% HNT loading) and their corresponding MA crosslinked specimens. All specimens were dried in an oven at 105°C for 12 h prior to conducting the test. All DSC analyses were performed under an inert atmosphere by flowing nitrogen at the rate of 50 mL/min, between −20 and 250°C and at a scanning rate of 10°C/min.

RESULTS AND DISCUSSION

HNT Individualization

Unlike other nanolayered clays that must be exfoliated, HNTs naturally occur as small cylinders which average 30 nm in diameter. The HNT specimen used in this research was unprocessed and hence the nanotubes within were clustered. This was confirmed from the SEM photomicrographs in a previously published report [8]. Therefore, many separation techniques were employed in this study to individualize HNT clusters. These techniques include: high speed mechanical stirring, ultrasonication, addition of non-ionic surfactant, and changing the solution pH.

Shear force from high speed mechanical stirring was used to effectively break down the HNT clusters. Ultrasonication generates intense and high frequency sound. The sound itself consists of regions of high and low pressure that move through a material as waves. As these waves pass through the liquid in the bath, each tiny portion of liquid vibrates back and forth in response to these pressure fluctuations which results in breaking of the clusters of HNTs [8].

Non-ionic surfactant Tween® 80 was used as a dispersant to improve the separation of HNTs [31]. The change of pH value is one of the key factors to separate HNTs. HNTs carry a negative charge on the basal or "face" surface of their crystals but the charge on crystal edges varies with the pH of the ambient environment. The amphoteric nature of the edge surface may be ascribed to the protonation and deprotonation of hydroxyl groups coordinated with exposed Al ions under acid and alkaline pH conditions, respectively [7]. It has been reported that at pH 7.5 and above, the HNTs tend to repel each other since the charge on both the edge and face surface is negative [32]. As a result, the system deflocculates, and loses cohesion. In this study, uniform and stable HNT dispersion was obtained after using these separation techniques sequentially. This stable HNT dispersion was used to prepare HNT–PVA nanocomposites.

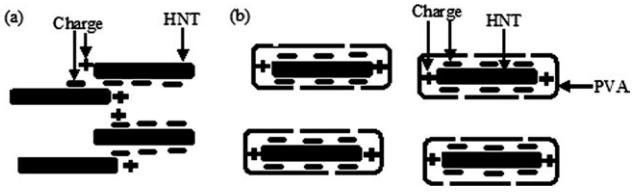

FIG. 1. HNT clustering (a) and PVA surrounded HNTs without clustering (b) in acidic environment.

Mechanism of Uniform HNT Dispersion in Acidic Crosslinking Condition

The individualized HNTs in dispersion can aggregate and deposit when pH value is changed to acidic values. However, after HNT dispersion was mixed with PVA solution, the aggregation did not occur for many days, even in acidic condition, during PVA crosslinking. This is possibly because the high viscosity of the PVA solution prevents them from coming closer due to the change of charges on edge surfaces of the HNTs in acidic environment. The surface of HNTs may be even wrapped by polymers. Earlier research has shown that polyaniline does wrap around HNTs. Silicone oil with polyaniline-wrapped HNTs dispersed in it was shown to have electrorheological properties [33]. Figure 1 shows a schematic of this mechanism. It shows individualized HNTs can aggregate with each other in acidic situation during opposite charge attracting. However, as mentioned earlier, high viscosity of PVA solution can help individualized HNTs to retard or even prevent aggregation by immobilizing them.

TEM and SEM Analysis of HNT Dispersion in PVA and Crosslinked PVA

Figure 2a–c shows typical TEM images of HNT–PVA nanocomposite and MA crosslinked HNT–PVA nanocomposite and SEM image of HNT–PVA nanocomposite surface, respectively. All nanocomposites had 10% HNT loading. Both TEM images clearly show that the HNTs were individualized and the uniformly dispersed within the PVA or crosslinked PVA. As mentioned earlier, high

 DOI 10.1002/pc

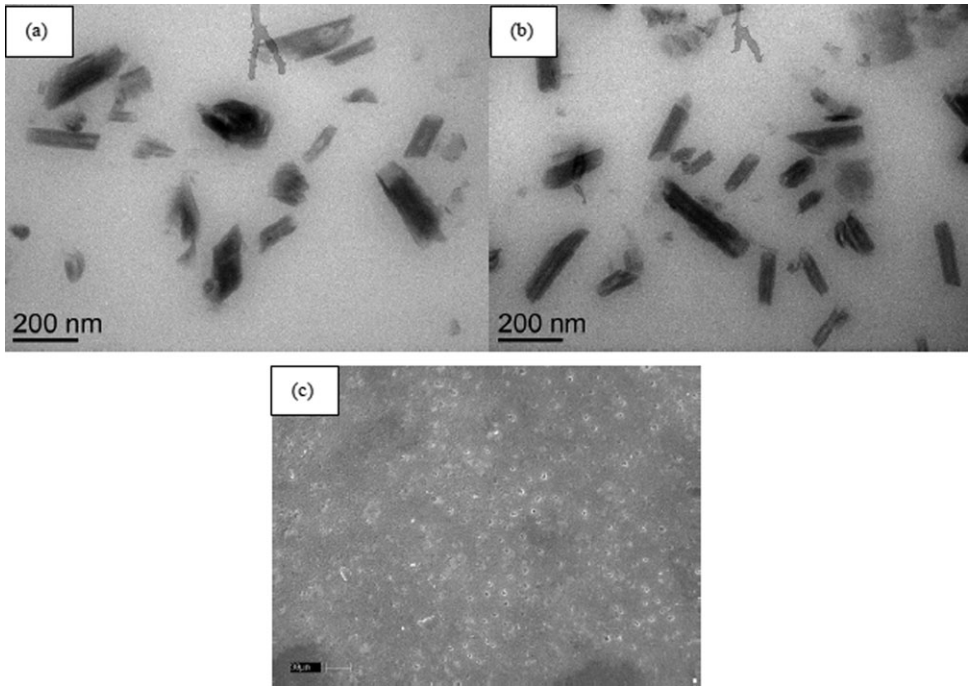

FIG. 2. TEM images of (a) HNT–PVA nanocomposite and (b) crosslinked HNT–PVA nanocomposite and SEM images of (c) HNT–PVA nanocomposite. All contain 10% HNT loading.

viscosity of the PVA solution can help individualized HNTs to retard or even prevent aggregation by immobilizing them. The degree or uniformity of dispersion of the HNTs within the polymer plays an important role on its mechanical properties [34]. Also, since the HNTs are uniformly dispersed, both mechanical and thermal properties of the nanocomposites would also be expected to be uniform [8]. The SEM image shows no obvious HNT aggregation at the surface of the HNT–PVA nanocomposite and that most of HNTs have been incorporated in the bulk of the PVA films.

Sol–Gel and Swelling Analyses

A study of crosslinking PVA with dicarboxylic acids, including MA, with sulfuric acid as a catalyst has been described earlier [29]. However, our preliminary study showed no difference in the extent of crosslinking between MA crosslinked PVA catalyzed by sulfuric acid and phosphoric acid. As a result, in all subsequent experiments, phosphoric acid was used as a catalyst to crosslink PVA and HNT–PVA nanocomposites because of its lower toxicity compared to sulfuric acid [27].

Sol–gel and swelling analyses were performed for noncrosslinked (control) and crosslinked PVA, as well as for the resin in the crosslinked HNT–PVA nanocomposites to evaluate the level of crosslinking. Table 1 presents the sol–gel and swelling results for MA crosslinked PVA as well as control PVA. The results show that the PVA gel (crosslinked component) percentages of the crosslinked PVA and the resin in the crosslinked HNT–PVA nanocomposites were 93.1 and 94.8%, respectively, while the control PVA dissolved completely during the sol–gel test. The high gel percentage suggests that the PVA was crosslinked by MA when catalyzed by phosphoric acid. The results also show that the swelling powers of crosslinked PVA and the resin in the crosslinked HNT–PVA nanocomposites were 52.3 and 51.0%, respectively, much lower than control (noncrosslinked) PVA (107.3%), further confirming the crosslinking.

ATR-FTIR Analysis

When MA is made to react with PVA, the carboxylic groups (COOH) in MA react with the hydroxyl groups (OH) in the PVA forming ester linkages. Figure 3A shows typical carboxylic ester linkages in MA crosslinked PVA. Figure 3B-a and b shows ATR-FTIR spectra for control HNT–PVA nanocomposite and MA crosslinked HNT–PVA nanocomposite. Since HNTs cannot crosslink with MA, ATR-FTIR spectra only indicate the chemical changes within the PVA resin in HNT–PVA nanocomposites before

TABLE 1. Sol–gel and swelling power results of PVA and MA crosslinked PVA.

Tests	Control PVA	Crosslinked PVA	PVA in crosslinked HNT–PVA[a] nanocomposites
Gel percentage (%)	0	93.1 (8.3)[b]	94.8 (7.2)
Swelling power (%)	107.3 (5.2)	52.3 (9.2)	51.0 (8.0)

[a] 10% HNT.
[b] Values in the parentheses are % coefficient of variation.

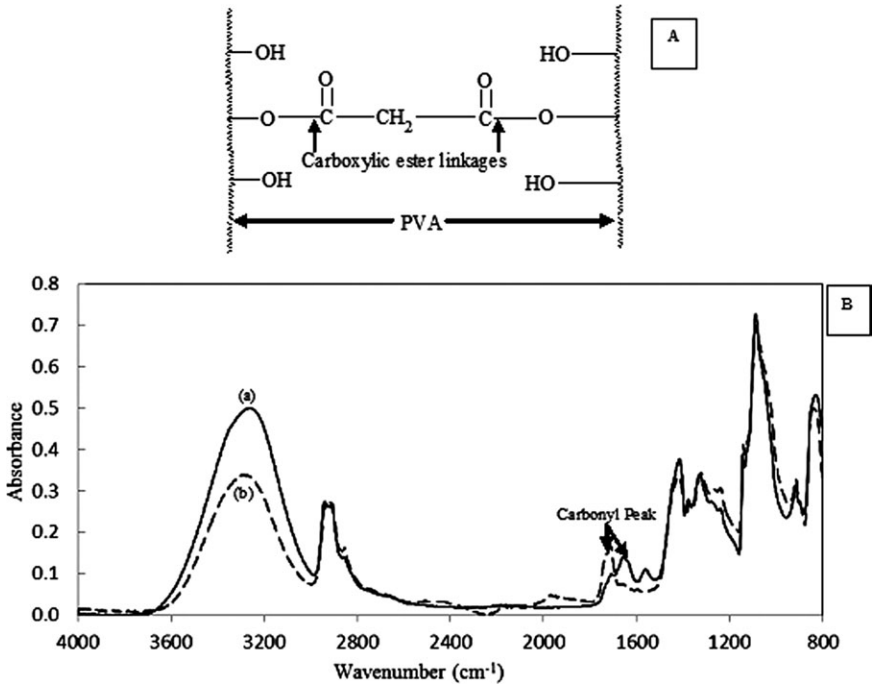

FIG. 3. A: Schematic of the carboxylic ester linkage in MA crosslinked PVA structure; B: ATR-FTIR spectra of (a) HNT–PVA nanocomposite and (b) MA crosslinked HNT–PVA nanocomposite. Both contain 10% HNT loading.

and after crosslinking. A broad band at 3500–3200 cm^{-1} wavenumber seen in both spectra is a result of the O–H stretching vibration resulting from the strong intra-molecular and inter-molecular hydrogen bonding [35–37]. The absorption band observed between 3000 and 2820 cm^{-1} wavenumbers is due to the stretching of aliphatic C–H bonds [36]. The absorbance intensity ratio for O–H to C–H bands showed a decrease from 1.82 in spectrum (a) for control PVA compared to 1.23 for spectrum (b) for crosslinked PVA. This lower absorption clearly indicates a reduction in the O–H groups and confirms the crosslinking of PVA by MA [36]. Absorption at 1750–1650 cm^{-1} (stretching of C=O) for noncrosslinked specimen [spectrum (a)] was weak (intensity ratio of C=O to C–H = 0.50) and indicates the presence of carbonyl (C=O) in the nanocomposites from the nonhydrolyzed acetate group remaining in the PVA (98–99% hydrolyzed), confirming the earlier results obtained by Gohil et al. [35] and Mansur et al. [36]. In the ATR-FTIR spectrum (b), however, a slightly sharp absorption (intensity ratio of C=O to C–H = 0.61) observed at 1750–1650 cm^{-1} wavenumber indicates presence of C=O in the crosslinked PVA of the nanocomposites as expected. This shows that in addition to the nonhydrolyzed vinyl acetate groups, some residual unreacted carboxylic groups from MA and carboxylic ester groups (Fig. 3A) from crosslinked PVA also exist in the crosslinked HNT–PVA nanocomposites, both contributing to the stronger C=O absorption.

Overall, the ATR-FTIR results indicate that the PVA in HNT–PVA nanocomposites were crosslinked based on the decreased intensity of bands for O–H stretching vibration combined with the increased intensity of bands for C=O stretching vibrations.

Tensile Properties and Moisture Content

Table 2 presents tensile test results and moisture content values for pure (control) PVA and noncrosslinked HNT–PVA nanocomposites with HNT loading from 5% to 20% and their MA crosslinked specimens. The Young's modulus value for the control PVA was 245 MPa. The Young's modulus value for the HNT–PVA nanocomposites were higher than that obtained for control PVA and increased with the HNT loading, as was expected. For nanocomposites with 5 and 10% HNT loading, the Young's moduli were 286 and 388 MPa, respectively, and when the HNT loading increased to 20% the Young's modulus increased to 466 MPa, about two times that of control PVA. This phenomenon is commonly observed for most polymers loaded with inorganic nanoparticles due to the increased tortuosity of the polymer molecules, significantly harder nanoparticles, and increased nanoparticle–polymer interface [1, 38–43]. The facture stress for the control PVA was 34.3 MPa. The fracture stress values for HNT–PVA nanocomposites with 5 and 10% HNT loading were 29.1 and 27.7 MPa, respectively, and decreased to 22.0 MPa when the HNT loading increased to 20%, respectively. This is attributed to the significantly reduced fracture strain values brought about by HNT agglomeration in some areas of the nanocompo-

 DOI 10.1002/pc

TABLE 2. Tensile properties and moisture content for PVA, HNT–PVA nanocomposites, and their corresponding MA crosslinked specimens.

Specimens	Young's modulus (MPa)	Fracture stress (MPa)	Fracture strain (%)	Moisture content (%)
PVA	245 (20.6)[a]	34.3 (13.6)	336 (10.1)	9.2 (5.3)
Crosslinked PVA	1023 (19.1)	46.4 (8.5)	186 (30.2)	6.3 (7.6)
HNT–PVA (5% HNTs)	286 (16.2)	29.1 (8.7)	297 (32.1)	8.0 (5.6)
HNT–PVA (10% HNTs)	388 (17.0)	27.7 (9.8)	268 (22.9)	7.4 (1.0)
HNT–PVA (20% HNTs)	466 (11.3)	22.0 (10.7)	159 (34.8)	6.6 (1.0)
Crosslinked HNT–PVA (5% HNTs)	1105 (10.4)	42.1(9.5)	110.0 (22.3)	6.2 (4.2)
Crosslinked HNT–PVA (10% HNTs)	1185 (24.7)	38.8 (9.6)	74.9 (17.6)	6.0 (8.8)
Crosslinked HNT–PVA (20% HNTs)	1244 (0.4)	36.1 (0.6)	8.8 (22.9)	6.0 (6.1)

[a] Values in the parentheses are % coefficient of variation values.

sites, particularly at 20% loading, again, a phenomenon seen in most polymers. However, lower fracture strain may also be a result of the weaker bonds between the nanoparticles (HNTs) and PVA as noted by other researchers [44]. The fracture strain for control PVA was 336%. As seen from data in Table 2, fracture strains for the HNT–PVA nanocomposites are much lower than that obtained for control PVA and decreased as the HNT loading increased. The reduced fracture strain as a function of nanoparticle loading has been observed by many for other polymer nanocomposites [40]. The moisture content for control PVA was 9.2%, whereas for HNT-PVA nanocomposites with 5, 10, and 20% HNT loading the moisture content values were 8.0, 7.4, and 6.6%, respectively. This is because moisture content of HNTs is around 1.6%, lower than PVA.

The Young's moduli of the MA crosslinked PVA and MA crosslinked HNT–PVA nanocomposites with 5, 10, and 20% HNT loading increased to 1023, 1105, 1185, and 1244 MPa, respectively, from 245 MPa for control PVA and from 286, 388, and 466 MPa for noncrosslinked HNT–PVA nanocomposites with the corresponding HNT loading. It is obvious that the increase in Young's modulus for the crosslinked PVA and HNT–PVA nanocomposites is solely due to the crosslinking of PVA which makes it rigid [45]. The reduction in moisture content from 9.2% for the noncrosslinked PVA to 6.3% after crosslinking and from 8.0%, 7.4 and 6.6% for the noncrosslinked HNT–PVA nanocomposites with 5, 10, and 20% HNT loading, respectively, to 6.2, 6.0, and 6.0% for the crosslinked HNT–PVA nanocomposites with the corresponding HNT loading is also responsible, at least partially, for higher Young's modulus. With lower moisture content, i.e., less plasticization, the structure maintains its higher rigidity, or stiffness [46]. Crosslinking also increased fracture stress values of PVA from 34.3 to 46.4 MPa. For HNT–PVA nanocomposites with 5, 10, and 20% HNT loading the fracture stress values increased from 29.1, 27.7, and 22.0 MPa to 42.1, 38.8, and 36.1 MPa, respectively, after crosslinking. From data presented in Table 2, it is also clear that after crosslinking, fracture strain values of PVA and HNT–PVA nanocomposites are significantly lower, as expected [38, 39, 47, 48]. The fracture strains, particularly in the case of crosslinked nanocomposites decreased significantly with HNT loading. The decrease in fracture stress is closely related to the decreased fracture strains.

It should be noted that tensile properties of HNT–PVA nanocomposites and crosslinked HNT–PVA nanocomposites are comparable or higher than many traditional polymers, including polyethylene (Young's modulus: 800 MPa; fracture stress: 15 MPa), polypropylene (Young's modulus: 1900 MPa; fracture stress: 40 MPa), and nylon 6 (Young's modulus: 1800 MPa; fracture stress: 70 MPa) [49]. As a result, these PVA based biodegradable nanocomposites could easily replace many of these traditional plastic materials. Also, after crosslinking their moisture sensitivity decreases, making them more useful. Biodegradable plastics based on PVA can reduce the current landfilling load significantly.

Figure 4a and b shows typical stress versus strain plots of noncrosslinked HNT–PVA nanocomposite and MA crosslinked HNT–PVA nanocomposite, respectively. The HNT loading in both specimens was 10% by weight. Figure 4a shows HNT–PVA nanocomposite initially showed elastic behavior but then showed a plastic plateau (yielding) until reaching its fracture point. This plateau is due to PVA's high ductility. While stress versus strain plot for the crosslinked HNT–PVA nanocomposite shown in Fig. 4b also shows yielding, it shows no plastic deformation because of the crosslinking.

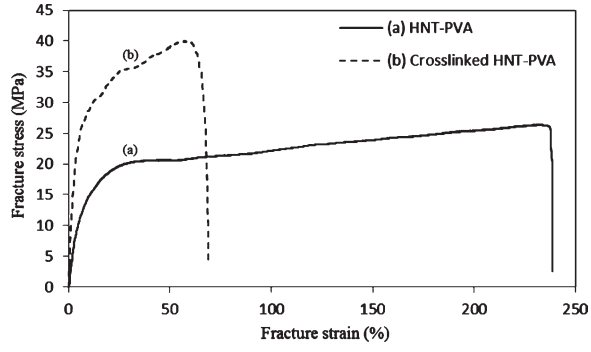

FIG. 4. Typical stress versus strain plots for (a) noncrosslinked HNT–PVA nanocomposite and (b) MA cross-linked HNT–PVA nanocomposite. Both contain 10% HNT loading.

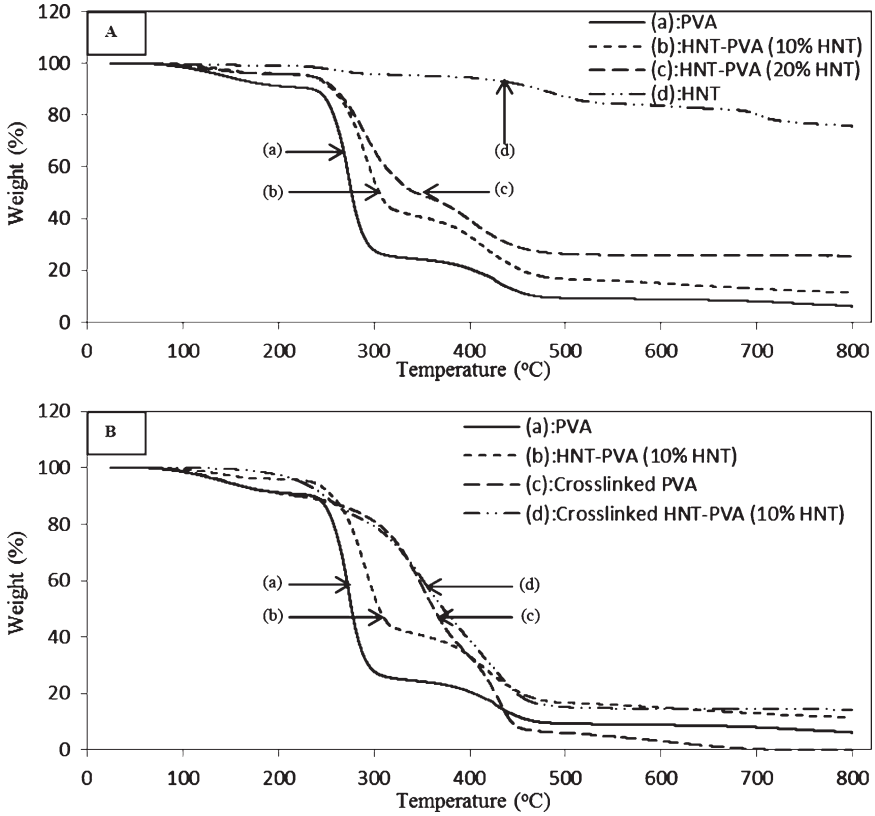

FIG. 5. Typical TGA thermograms A: (a) PVA, (b) HNT–PVA nanocomposite (10% HNT loading), (c) HNT–PVA nanocomposite (20% HNT loading), and (d) HNTs; B: (a) PVA, (b) HNT–PVA nanocomposite (10% HNT loading), (c) MA crosslinked PVA, and (d) MA crosslinked HNT–PVA nanocomposite (10% HNT loading).

Thermogravimetric Analysis

Figure 5A presents typical TGA thermograms of PVA, HNT–PVA nanocomposites (10 and 20% HNT loading) and HNTs. Thermogram 5A (a) for control PVA shows two decomposition onset temperatures (T_{d1}) and (T_{d2}), at 255 and 390°C, respectively. Weight losses for the PVA were 30% at 266°C, 50% at 276°C and up to 94% at 800°C. Two-step degradation of PVA has been reported earlier by Peng and Kong [50]. A likely explanation for this is that PVA first degrades into smaller molecular weight polymer at around 250°C by chain scission and degrades further into carbon char at temperatures above 350°C. Results of this study confirm the earlier findings [50]. Thermograms 5.5A (b) and (c) for HNT–PVA nanocomposites, with 10 and 20% HNT loading, respectively, also show two decomposition onset temperatures. However, their T_{d1} and T_{d2} at 260 and 393°C, respectively, are 3–5°C higher than those observed for PVA. While these changes are small they confirm the higher thermal stability due to the addition of HNTs. Weight losses observed for the HNT–PVA nanocomposites (10% HNT loading) were 30% at 286°C, 50% at 305°C, and 88% at 800°C. Weight losses observed for the HNT-PVA nanocomposites (20% HNT loading) were 30% at 295°C, 50% at 343°C (both temperatures are higher than those obtained for HNT–PVA nanocomposites with 10% HNT loading), and 74% at 800°C. These data confirm the higher thermal stability of the HNT–PVA nanocomposites. Thermogram 5A (d) for HNTs showed no sharp thermal degradation. Weight losses observed for pure HNTs were 10% at 471°C, 20% at 700°C, and 24% at 800°C, confirming higher thermal stability of HNTs [13]. Thus it is obvious that HNT loading is responsible for the higher thermal stability of the HNT–PVA nanocomposites.

Figure 5B presents typical TGA thermograms of PVA, HNT–PVA nanocomposite (10% HNT loading) and their corresponding MA crosslinked specimens. Thermograms 5.5B (a) and 5.5B (b) are for PVA and HNT–PVA nanocomposites, respectively, and have been described in the last paragraph. Thermogram 5B (c), for crosslinked PVA, also shows a two-step degradation pattern with T_{d1} and T_{d2} (no so obvious) observed at 305 and 417°C, respectively. However, the steps are not as distinct when compared to the control PVA. The weight losses observed were 30% at 329°C, 50% at 362°C, and almost 100% at 800°C. These results indicate that the crosslinked PVA has significantly higher thermal stability compared to control PVA in the range of 240–430°C. Increased thermal stability after crosslinking has been observed earlier for many polymers [51–53]. It was also observed that the

 DOI 10.1002/pc

final residual percentage for MA crosslinked PVA was lower than pure PVA. This is partially because of the unreacted crosslinker (MA) and crosslinking agent (phosphoric acid) that remain trapped in the HNT–PVA nanocomposites. During the TGA test these compounds are removed at a relatively lower temperature. Thermogram 5B (d) for crosslinked HNT–PVA nanocomposites also shows a single step degradation with T_d observed at 380°C. Weight losses observed were 30% at 329°C, 50% at 372°C, and 86% at 800°C. As is expected, these values are close to those obtained for the crosslinked PVA, the major constituent in the nanocomposite. These results clearly indicate that crosslinking of PVA using MA can increase its thermal stability as well as that of HNT–PVA nanocomposites in addition to enhancing their tensile properties.

Differential Scanning Calorimetry

Typical DSC thermograms for PVA and MA crosslinked PVA are presented in Fig. 6A. Thermogram 6A (a) for control PVA shows T_g and T_m of 92.0 and 196.1°C, respectively. The ΔH_f of 81.1 J/g, compared to 138.6 J/g for 100% crystalline PVA resulted in a crystallinity of 58.5% for control (pure) PVA [54–57]. Thermogram 6A (b) for the crosslinked PVA shows T_g and T_m of 102.1 and 189.7°C, respectively. The ΔH_f and the crystallinity of the crosslinked PVA were 36.8 J/g and 26.6%, respectively. The lower ΔH_f and higher T_g further confirm that the PVA was effectively crosslinked by MA. The higher T_g and lower crystallinity after crosslinking are due to restricted segmental motion of the molecules and are commonly observed phenomena in most polymers [1, 54, 58, 59].

Figure 6B presents typical DSC thermograms of (a) HNT–PVA nanocomposite and (b) MA crosslinked HNT–PVA nanocomposite. The T_g and T_m for the HNT–PVA nanocomposites were observed at 90.5 and 201.9°C, respectively. The change in T_g for nanocomposite is insignificant. While the T_m value is about 5°C higher than that of control PVA, the T_g is about 1.5°C lower. This suggests that HNTs have the ability to lead to decrease T_g and increase T_m of polymers [21, 60]. Nakamura et al. [18] also observed similar decrease in T_g as a result of HNT addition. They argued that this was a result of free volume addition. The ΔH_f and the crystallinity of the PVA in HNT–PVA nanocomposites (10% loading) were 43.3 J/g and 31.2%, respectively, which were much lower than 85.9 J/g and 62.0%, respectively, obtained for control PVA. It is likely that the HNTs can inhibit the crystallization of PVA, as they are well dispersed [61]. However, higher T_m suggested that the average crystal size in nanocomposites was larger. Thermogram 6B (b) is for MA crosslinked HNT–PVA composites but mainly represents crosslinked PVA behavior. The T_g and T_m observed were 99.0 and 191.9°C, respectively, and confirm earlier observations that MA crosslinking can

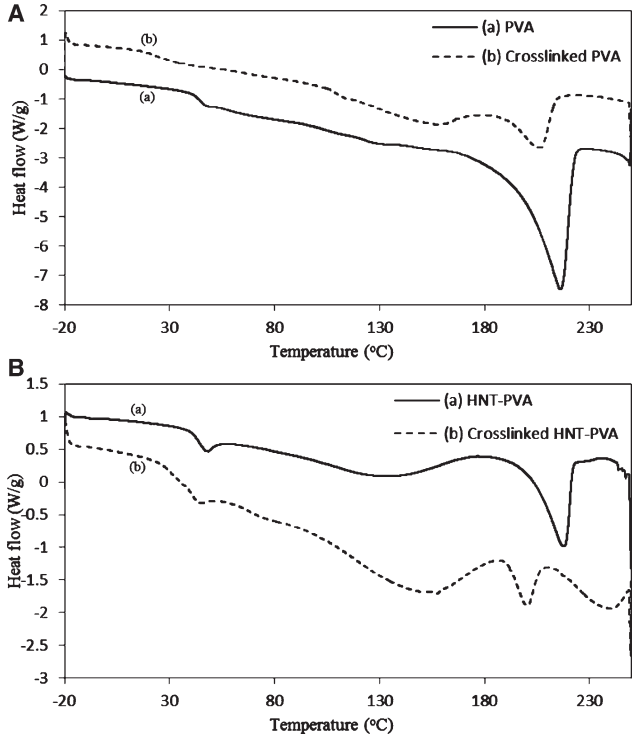

FIG. 6. DSC thermograms A: (a) PVA and (b) MA crosslinked PVA; B: (a) HNT–PVA nanocomposite and (b) MA crosslinked HNT–PVA nanocomposite. Both contain 10% HNT loading.

increase T_g and decrease T_m of PVA. These changed characteristics are reflected in the crosslinked HNT–PVA nanocomposites. The ΔH_f and crystallinity of PVA in crosslinked HNT–PVA nanocomposites were 8.6 J/g and 6.2%, respectively. These are significantly lower than those for the PVA in HNT–PVA nanocomposites and the MA crosslinked PVA, showing the combined effect of crosslinking and the ability of the HNTs to restrain the molecular motion needed for crystallization.

CONCLUSIONS

The biodegradable membrane-like HNT–PVA nanocomposites with differing HNT loadings were produced using blending and casting methods. Several separation techniques such as mechanical stirring, ultrasonication, non-ionic surfactant, and desired solution pH, were used to individualize HNTs and obtain stable HNT dispersion. The TEM images indicated that HNTs were uniformly dispersed in both PVA and MA crosslinked PVA. ATR-FTIR results confirmed that PVA can be crosslinked using MA as crosslinker and phosphoric acid as catalyst. MA crosslinked PVA was highly water-insoluble with decreased swelling ability. PVA and HNT–PVA nanocomposites showed higher mechanical properties and thermal stability after crosslinking. HNT loading also was responsible for higher thermal stability of the PVA based nanocomposites. Fracture strain also decreased with HNT loading for both crosslinked and noncrosslinked PVA.

The DSC results indicated that HNT loading decrease T_g as well as crystallinity while increasing the T_m of PVA. Crosslinking of PVA resulted in higher T_g, lower T_m, and lower crystallinity as was expected.

ACKNOWLEDGMENTS

The authors would like to thank the Cornell Center for Materials Research (CCMR) for the use of their facilities.

REFERENCES

1. R. J. Young and P. A. Lovell PA, *Introduction to Polymers*, 3rd ed, CRC Press, Boca Raton, FL, 591 (2011).
2. G. Cao and Y. Wang, *Nanostructures and Nanomaterials: Synthesis, Properties, and Applications*, 2nd ed, World Scientific, Singapore, 61 (2011).
3. K.M. Dean, E. Petinakis, and L. Yu, "Biodegradable Thermoplastic Starch/Poly(vinyl alcohol) Nanocomposites with Layered Silicates," in *Nanocomposites with Biodegradable Polymers: Synthesis, Properties and Future Perspectives*, Oxford University Press, Oxford, UK, 58 (2011).
4. P. Lu, M. Zhang, P. Qian, and Q. Zhu, *Polym. Compos.*, **33**, 889 (2012).
5. J.Y. Kim, H.J. Choi, C.S. Kang, and S.H. Kim, *Polym. Compos.*, **31**, 858 (2010).
6. M. Liu, B. Guo, M. Du, and D. Jia, *Appl. Phys. A*, **88**, 391 (2007).
7. E. Joussein, S. Petit, J. Churchman, B. Theng, D. Righi, and B. Delvaux, *Clay Miner.*, **40**, 383 (2005).
8. P. Rathi, *Soy Protein based Nanophaser Reins for Green Composites, A Project Report*, Cornell University, Ithaca, NY, 13 (2007).
9. M. Liu, B. Guo, M. Du, X. Cai, and D. Jia. *Nanotechnology*, **18**, Art. No.: 455703 (2007).
10. Y. Ye, H. Chen, J. Wu, and L. Ye, *Polymer*, **48**, 6426 (2007).
11. S. Deng, J. Zhang, L. Ye, and J. Wu, *Polymer*, **49**, 5119 (2008).
12. N. Ning, Q. Yin, F. Luo, Q. Zhang, R. Du, and Q. Fu, *Polymer*, **48**, 7374 (2007).
13. M. Du, B. Guo, and D. Jia, *Eur. Polym. J.*, **42**, 1362 (2006).
14. D.C.O. Marney, L.J. Russell, D.Y. Wu, T. Nguyen, D. Cramm, N. Rigopoulos, N. Wright, and M. Greaves, *Polym. Degrad. Stab.*, **93**, 1971 (2008).
15. M. Du, B. Guo, Y. Lei, M. Liu, and D. Jia. *Polymer*, **49**, 4871 (2008).
16. B. Guo, Y. Lei, F. Chen, X. Liu, M. Du, and D. Jia, *Appl. Surf. Sci.*, **255**, 2715 (2008).
17. P. Pasbakhsh, H. Ismail, M.N.A. Fauzi, and A.A. Bakar, *Appl. Clay Sci.*, **48**, 405 (2010).
18. R. Nakamura, A.N. Netravali, and M. Hosur, *J. Adhes. Sci. Technol.*, **26**, 1295 (2012).
19. R. Nakamura, A.N. Netravali, A.B. Morgan, M.R. Nyden, and J.W. Gilman, *Fire Mater.*, DOI: 10.1002/fam.2113 (2012).
20. E.S. Stevens, *Green Plastics: An Introduction to the New Science of Biodegradable Plastics*, Princeton University Press, Princeton, NJ, 10 (2002).
21. K. Prashantha, M.F. Lacrampe, and P. Krawczak, *Express Polym. Lett.*, **5**, 295 (2011).
22. W.Y. Zhou, B. Guo, M. Liu, R. Liao, A.B.M. Rabie, and D. Jia, *J. Biomed. Mater. Res. A*, **93**, 1574 (2010).
23. Thermo Scientific, *Thermo Scientific Pierce-Crosslinking Technical Handbook*, http://www.piercenet.com/files/1601673_Crosslink_HB_Intl.pdf (2011).
24. C.K. Yeom and K.H. Lee, *J. Membrane Sci.*, **109**, 257 (1996).
25. Y. Zhang, P.C. Zhu, and D. Edgren, *J. Polym. Res.*, **17**, 725 (2010).
26. BASF, *Glyoxal as a Cellulose Crosslinker*, http://www.intermediates.basf.com/chemicals/glyoxal/crosslinker-for-cellulose (2011).
27. MSDS, http://www.msdsonline.com (2011).
28. N. Weiner, *Org. Synth., Collective* **2**, 376 (1943).
29. S. Jian and S.X. Ming, *Desalination*, **62**, 395 (1987).
30. S. Majumdar and B. Adhikari, *Sensors Actuat. B Chem.*, **114**, 747 (2006).
31. N. Karatepe, *Energ. Convers. Manag.*, **44**, 1275 (2003).
32. G.J. Churchman and B.K.G. Theng, *Clay Miner.*, **19**, 161 (1984).
33. W.L. Zhang and H.J. Choi. *Colloid Polym. Sci.*, DOI 10.1007/s00396-012-2719-6 (2012).
34. K. Yano, A. Usuki, and A. Okada, *J. Polym. Sci. Polym. Chem.*, **35**, 2289 (1997).
35. J.M. Gohil, A. Bhattacharya, and P. Ray, *J. Polym. Res.*, **13**, 161 (2006).
36. H.S. Mansur, C.M. Sadahira, A.N. Souza, and A.A.P. Mansur, *Mater. Sci. Eng. C*, **28**, 539 (2008).
37. J.H. Kim, E.J. Moon, and C.K. Kim, *J. Membr. Sci.*, **216**, 107 (2003).
38. Y. He, W. Kong, W. Wang, T. Liu, Q. Gong, and J. Gao, *Carbohydr. Polym.*, **87**, 2706 (2012).
39. R.A. Vaia, K.D. Jandt, E.J. Kramer, and E.P. Giannelis, *Chem. Mater.*, **8**, 2628 (1996).
40. H. Kumar, M. Hosur, and A.N. Netravali, *J. Adhes. Sci. Technol.*, **24**, 217 (2010).
41. C. Lew, F. Choudhury, M. Hosur, and A.N. Netravali, *J. Adhes. Sci. Technol.*, **21**, 1407 (2007).
42. U. Chatterjee, S.K. Jewrajka, and S. Guha, *Polym. Compos.*, **30**, 827 (2009).
43. J. Fu, L. Chen, H. Yang, Q. Zhong, L. Shi, W. Deng, X. Dong, Y. Chen and G. Zhao, *Polym. Compos.*, **33**, 404 (2012).
44. D. Zhao, Y. Zhang, H. Gong, B. Zhu, and X. Zhang, *J. Nanomater.*, Art. ID **246847** (2011).
45. L. Zhang, P. Chen, J. Huang, G. Yang, and L. Zheng, *J. Appl. Polym. Sci.*, **88**, 422 (2003).
46. J. Zhang, P. Mungara, and J. Jane, *Polymer*, **42**, 2569 (2001).
47. M. Bengtsson, K. Oksman, and N.M. Stark, *Polym. Compos.*, **27**, 184 (2006).
48. F. Zhao, Xu. Qin, and S. Feng, *Polym. Compos.*, **33**, 44 (2012).
49. Tensile property testing of plastics - MatWeb. http://www.matweb.com/reference/tensilestrength.aspx (2010).
50. Z. Peng and L.X. Kong, *Polym. Degrad. Stab.*, **92**, 1061 (2007).

51. S. Chabba, G.F. Matthews, and A.N. Netravali, *Green Chem.*, **7**, 576 (2005).
52. F.T. Rodrigues, V.C.A. Martins, and A.M.G. Plepis, *Polimeros*, **20**, 92 (2010).
53. B.S. Liu, C.H. Yao, and S.S. Fang, *Macromol. Bioscience*, **8**, 432 (2008).
54. S.B. Warner, *Fiber Science*, Prentice Hall, Upper Saddle River, NJ, 205 (1995).
55. R.L. Blaine (TA Instruments), *Determination of Polymer Crystallinity by DSC*, www.tainstruments.com/library_download.aspx?file=TA123.PDF (2011).
56. W.J. Sichina (PerkinElmer Instruments). *DSC as Problem Solving Tool: Measurement of Percent Crystallinity of Thermoplastics*, http://www.perkinelmer.com/Content/applicationnotes/app_thermalcrystallinitythermoplastics.pdf (2011).
57. O.W. Guirguis and M.T.H. Moselhey, *Nature Sci.*, **4**, 57 (2012).
58. J.H. Kim, J.Y. Kim, Y.M. Lee, and K.Y. Kim, *J. Appl. Polym. Sci.*, **45**, 1711 (1992).
59. T.N. Mtshali, I. Krupa, and A.S. Luyt, *Thermalchim. Acta.*, **380**, 47 (2001).
60. M. Liu, B. Guo, M. Du, F. Chen, and D. Jia, *Polymer*, **50**, 3022 (2009).
61. A. Boudenne, L. Ibos, Y. Candau, and S. Thomas, *Handbook of Multiphase Polymer Systems*, Wiley, Chichester, West Sussex, UK, 455 (2011).